# Importance of Recombination at the TCO/Electrolyte Interface for High Efficiency Quantum Dot Sensitized Solar Cells

**ARTICLE** *in* THE JOURNAL OF PHYSICAL CHEMISTRY C · JULY 2012

Impact Factor: 4.77 · DOI: 10.1021/jp306782q



**4 AUTHORS**, INCLUDING:

Sven Rühle
Xjet 3D
**47** PUBLICATIONS **2,391** CITATIONS
SEE PROFILE

Arie Zaban
Bar Ilan University
**170** PUBLICATIONS **10,728** CITATIONS
SEE PROFILE

THE JOURNAL OF PHYSICAL CHEMISTRY C

Article

pubs.acs.org/JPCC

# Importance of Recombination at the TCO/Electrolyte Interface for High Efficiency Quantum Dot Sensitized Solar Cells

Sven Rühle,*[,†] Shay Yahav,[†] Shlomit Greenwald, and Arie Zaban*

Department of Chemistry, Center for Nanotechnology & Advanced Materials, Bar Ilan University, Ramat Gan 52900, Israel

Supporting Information

**ABSTRACT:** Here, we show that, in CdSe quantum dot sensitized solar cells (QDSCs), recombination of electrons from the transparent conducting oxide (TCO) front electrode with oxidized species of the polysulfide redox electrolyte cannot be neglected like in dye-sensitized solar cells (DSCs). We demonstrate that light to electric power conversion efficiencies up to 4% can be achieved when recombination at the front electrode is suppressed by a compact $TiO_2$ layer deposited in between the TCO substrate and the QD sensitized porous $TiO_2$ film. Numerical simulations based on a simple equivalent circuit suggest that, over a wide potential range, electron transfer into the electrolyte at the TCO substrate is the dominant recombination path, which is usually not considered, suggesting that the current understanding of QDSCs has to be revised.

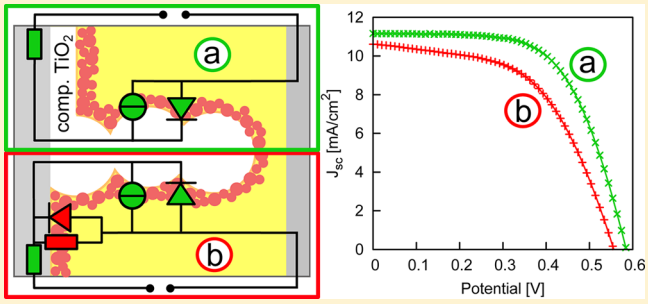


## INTRODUCTION

Over the last years, quantum dot sensitized solar cells (QDSCs) have shown a steady increase in their light to electric power conversion efficiency. QDSCs are based on a porous wide bandgap semiconductor (mostly $TiO_2$) that is deposited onto a transparent conducting substrate such as fluorine-doped $SnO_2$ (FTO). QDs deposited inside the pores absorb light and inject electrons from their excited state into the conduction band of the porous film while a redox electrolyte recharges the oxidized QD and transports the positive charge to the back electrode.[1] QDs are attractive light absorbers due to their size dependent absorption spectrum that can be easily controlled by QD growth conditions.[2−4] Record efficiencies above 4% have been reported (on cells <1 $cm^2$) with CdSe QD sensitized mesoporous $TiO_2$ films immersed in aqueous polysulfide redox electrolyte.[5−7]

The working principle of QDSCs is very similar to that of DSCs where the low light absorption of a thin absorber layer is compensated by an up to 3 orders of magnitude enhanced microscopic surface area inside the porous electrode. Consequently, recombination takes place at the large $TiO_2$/QD/electrolyte interface area and significant efforts were made to suppress the recombination mechanism. While for DSCs coatings[8−10] and surface treatments[11,12] have been investigated to prevent electrons from recombining with oxidized redox species, it was found in QDSCs that a ZnS post-treatment following QD deposition strongly improves the cell performance.[13−16] Recent research concluded that the ZnS treatment mainly reduces the recombination by passivating the CdSe QDs rather than the $TiO_2$ surface.[17]

Electron transfer from the FTO substrate into the electrolyte is an alternative recombination path that has not received much attention in QDSCs. Even though the FTO/electrolyte interface area is orders of magnitude smaller compared to the porous $TiO_2$/electrolyte interface, the electrocatalytic activity of FTO in redox electrolyte can be substantial, partly due to the lower conduction band edge of FTO compared to $TiO_2$ that leads to an increased overlap of electronic conduction band states with oxidized species of the electrolyte. In liquid electrolyte DSCs, extensive research was carried out to investigate the recombination at the FTO front electrode, and compact $TiO_2$ layers were deposited to cover the FTO substrate. For $I^-/I_3^-$ redox electrolyte based cells, it was found that the compact layer does not lead to a significant improvement of the conversion efficiency due to a reduced blocking behavior at potentials approaching the maximum power point[18] but that such a layer is essential for quantitative electron lifetime studies.[19,20] In contrast, alternative redox couples or solid-state hole conductors require a compact blocking layer to suppress recombination at the FTO/hole conductor interface.[21] In QDSCs, compact layers have been used in conjunction with the $Fe(CN)_6^{3-}/Fe(CN)_6^{4-}$ redox couple with its fast charge transfer kinetics to prevent direct contact with the FTO substrate.[22] For polysulfide electrolyte-based QDSCs, it was shown that, in CdS sensitized cells, a compact blocking layer can improve the cell performance, even though the conversion efficiency remained low.[23] In CdS/CdSe sensitized cells, a significant increase in the conversion efficiency up to 3.85% was reported together with an improved cell stability.[24] In $ZrO_2$-based QDSCs, a compact $ZrO_2$ layer

Received: July 9, 2012
Revised: July 29, 2012
Published: July 30, 2012

   dx.doi.org/10.1021/jp306782q | J. Phys. Chem. C 2012, 116, 17473−17478

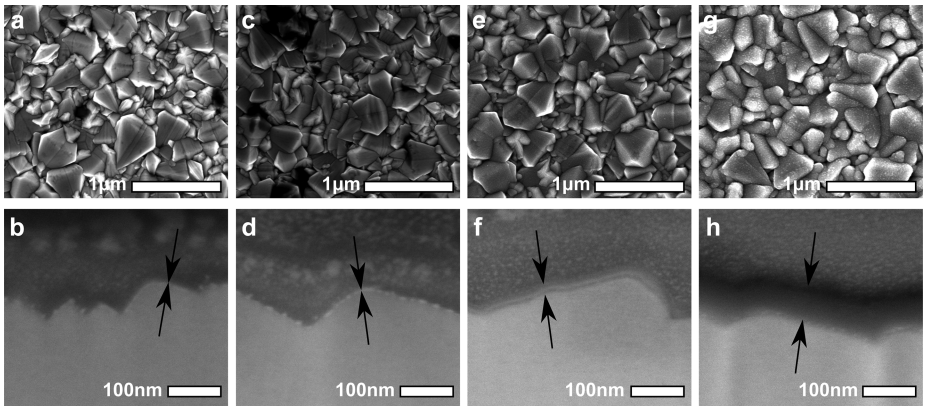


**Figure 1.** SEM top view and cross-section images (prepared by focused ion beam, FIB) of (a,b) bare FTO substrate (TEC 8), (c,d) after $TiCl_4$ treatment, (e,f) after one spray pyrolysis cycle, and (g,h) after four spray pyrolysis cycles. The morphology of the underlying FTO substrate remains visible in all images. For the $TiCl_4$ treated sample (d), no layer formation is visible in the cross-section image while the arrows in panels f and h emphasize the $TiO_2$ layer thickness.

was used to prevent direct contact between CdSe QDs and the FTO substrate to provide experimental evidence for electron injection from the QDs into the $ZrO_2$.[25]

Here, we show that a compact $TiO_2$ layer deposited in between the FTO substrate and the mesoporous $TiO_2$ film significantly improves the $J_{sc}$, $V_{oc}$, fill factor, and, ultimately, the light to electric power conversion efficiency $\eta$ of CdSe QDSCs. The improvement due to the compact layer is more pronounced in QDSCs that were prepared without the ZnS post-treatment, while higher absolute conversion efficiencies up to 4.0% were achieved with a compact layer in ZnS treated cells. All measurements were performed on cells with an illuminated cell area of 1.03 $cm^2$. On the basis of an equivalent circuit that describes recombination at the FTO substrate and the porous $TiO_2$ network by separate elements, we analyzed the $I-V$ characteristics. The results suggest that, in cells without a compact $TiO_2$ layer, electron transfer from the FTO substrate into the polysulfide electrolyte is the dominant recombination path at all voltages, while in cells with a compact $TiO_2$ layer, this recombination path is effectively blocked at photovoltages approaching the maximum power point.

## EXPERIMENTAL SECTION

FTO covered glass substrates with a sheet resistance of 8 Ω/square (Hartford) were thoroughly washed with soap, rinsed with ethanol and deionized water, and dried in a dry air stream. Spray pyrolysis of compact $TiO_2$ layers was carried out in a homemade $x-y$ scanning system where the thickness of the compact layer was controlled by the number of spray cycles. A hot plate (Harry Gestigkeit GmbH) was used to heat the FTO substrates to 450 °C, while a precursor solution of 0.1 M titaniumtetraisopropoxide and 0.2 M acetylaceton in ethanol was sprayed by a pneumatic nozzle (Spraying Systems Co.) onto the substrates.

For the preparation of QDSCs, a mesoporous $TiO_2$ film was deposited onto the FTO/compact $TiO_2$ substrates by the doctor blade method using commercial paste of $TiO_2$ nanoparticles with an average diameter of 100 nm (Solaronix). The films were annealed at 275 °C (30 min) and 375 °C (15 min) before they were sintered in air at 450 °C for 60 min. To sensitize the $TiO_2$ electrodes, a CdS seeding layer was deposited by the successive ionic layer adsorption and reaction method (SILAR) using four deposition cycles. In each cycle, the porous $TiO_2$ electrode was dipped in 0.1 M aqueous $CdClO_4$, deionized water, 0.1 M $Na_2S$, and again into deionized water for 1 min each.

Chemical bath deposition (CBD) of the CdSe absorber was subsequently used to sensitize the porous $TiO_2$ films.[26] Se powder was dissolved in a 200 mM $Na_2SO_3$ solution to form sodium selenosulphate (solution A). Aqueous solutions of 80 mM $CdSO_4$ and 120 mM of the trisodium salt of nitrilotriacetic acid ($N(CH_2COONa)_3$) were mixed in a 1:1 volume ratio (solution B) before solutions A and B were mixed in a 1:2 volume ratio. The porous $TiO_2$ electrodes were immersed into the final solution for 24 h at a temperature of 10 °C using a temperature controlled cooling bath. For the ZnS post-treatment, the CdSe-sensitized $TiO_2$ electrodes were dipped into a 0.1 M $Zn(CH_3COO)_2$ solution for 30 s, rinsed with deionized water, dipped into 0.1 M $Na_2S$ solution for 30 s, rinsed again, and dried in an air stream.

The blocking behavior of the compact layer was characterized by cyclic voltammetry in a three electrode setup with an Ag/AgCl reference electrode and a Pt counter electrode, using a redox electrolyte containing 0.01 M $K_3Fe(CN)_6$, 0.001 M $K_4Fe(CN)_6$, and 0.5 M KCl at pH 10 (adjusted with KOH).

$I-V$ characteristics were measured with an aqueous polysulfide redox electrolyte (1 M $Na_2S$, 0.1 M S, and 0.1 M NaOH)[25] using a Pb sheet covered with a PbS layer as a back electrode.[27] A class A solar simulator (Newport) with a light intensity of 100 mW/$cm^2$ was used to illuminate a solar cell area of 1.03 $cm^2$, while the $I-V$ characteristics were recorded with a potentiostat (Autolab) in a two electrode configuration, where the reference and counter electrode were connected to the Pb/PbS back electrode.

## RESULTS AND DISCUSSION

Compact $TiO_2$ layers were characterized using scanning electron microscopy (SEM) in conjunction with a focused ion beam (FIB). Figure 1a shows a SEM image of a commercial FTO substrate (TEC 8) before $TiO_2$ deposition. In the cross-section image, the high surface roughness can be seen where the arrows emphasize that no compact layer is deposited (Figure 1b). A FTO substrate treated with one $TiCl_4$ deposition cycle is shown in Figure 1c where the cross-section image shows some bright patches, which might be thin $TiO_2$ islands, but no clear layer formation could be detected (Figure


dx.doi.org/10.1021/jp306782q | J. Phys. Chem. C 2012, 116, 17473−17478

1d). The $TiCl_4$ treatment in which the TEC 8 substrate is immersed into concentrated $TiCl_4$ solution before it is sintered is often used to improve the mechanical contact between the mesoporous $TiO_2$ film and the FTO substrate. Consecutive cycles of $TiCl_4$ immersion followed by sintering might lead to the formation of a compact layer; however, spray pyrolysis is the more common procedure for covering FTO substrates. Figure 1e shows the substrate covered with a compact $TiO_2$ layer after one spray cycle where the polycrystalline morphology of the underlying FTO substrate remains clearly visible. In the cross-section image (Figure 1f), it can be seen that the $TiO_2$ layer is conformal, continuous, and covers the FTO substrate with a homogeneous film thickness of approximately 20 nm. Figure 1g shows a FTO substrate covered with a compact $TiO_2$ layer that was deposited by 4 spray cycles, while still retaining the underlying FTO morphology like in the previous case. The cross-section image shows a thickness of approximately 80 nm, which is conformal and homogeneous. Comparison with Figure 1f reveals that the layer thickness scales well with the number of spray cycles with a film thickness of ~20 nm per cycle.

Cyclic voltammetry measurements were used to characterize the quality of the compact $TiO_2$ layers, using a three electrode setup with an Ag/AgCl reference electrode and a Pt counter electrode. An aqueous electrolyte containing the $Fe(CN)_6^{3-}$/$Fe(CN)_6^{4-}$ redox couple at pH 10 was used to investigate the blocking behavior for electron transfer through the compact layer. Cyclic voltammetry is very sensitive to pinholes and thickness inhomogeneities and thus is a powerful tool for characterizing the quality of compact blocking layers. Figure 2a shows the cyclic voltammograms of the substrates in Figure 1, with strong oxidation and reduction peaks measured for the bare FTO substrate that are characteristic of efficient charge transfer across the FTO/electrolyte interface. The $TiCl_4$ treated FTO shows both peaks shifted to slightly different potentials, characteristic for slower reaction kinetics. This indicates that a $TiO_2$ layer has formed, which is too thin to prevent charge transfer or that $TiO_2$ patches cover only a fraction of the FTO surface, leaving a substantial area of the FTO uncovered. In contrast, a 20 nm thin $TiO_2$ layer deposited by spray pyrolysis suppresses the oxidation peak and shifts the reduction peak toward more negative potentials by several hundred millivolts. This onset is further shifted when the thickness of the compact layer is increased to ~80 nm.

The energy band diagram in Figure 2b schematically shows electron transfer from the FTO into the electrolyte, which is blocked by the compact $TiO_2$ layer due to the conduction band offset at the FTO/$TiO_2$ interface (Figure 2c). The strong suppression of charge transfer in the potential window from +700 mV down to −500 mV vs Ag/AgCl provides strong experimental evidence for a high quality conformal blocking layer that has a very low pinhole density, if any. The suppression of electron transfer at negative applied potential by compact $TiO_2$ layers is also observed for polysulfide electrolyte (see Supporting Information Figure S1).

The solar cell performance of CdSe QDSCs measured with an aqueous polysulfide redox electrolyte and a PbS counter electrode is presented in Figure 3. The $I-V$ characteristics of electrodes prepared without a ZnS post-treatment are shown in Figure 3a with a rather low photocurrent of the reference solar cell that was based on a sensitized porous $TiO_2$ film directly deposited onto an untreated FTO substrate. A substantial increase in the performance was observed when the bare FTO

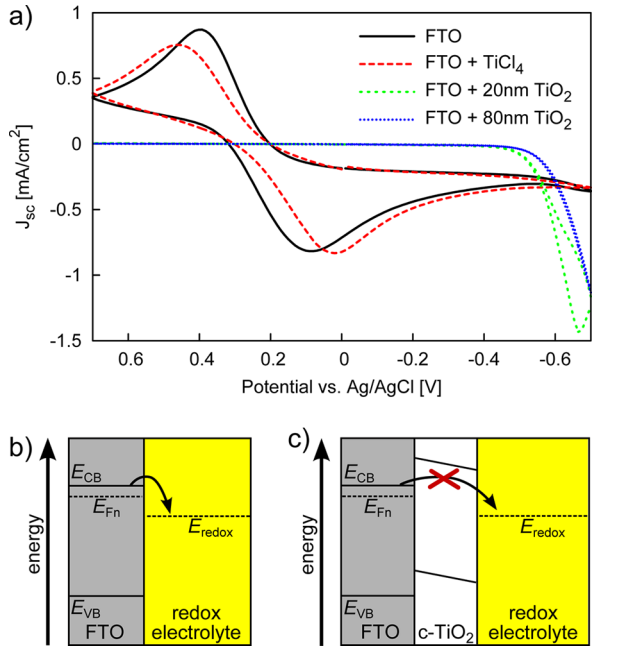


**Figure 2.** (a) Cyclic voltammetry measurements investigating the blocking behavior of $TiCl_4$ treated FTO (dashed red), FTO covered with 20 nm thick compact $TiO_2$ layer (short dashed green), and a FTO substrate covered with a 80 nm thick compact $TiO_2$ layer (dotted blue), compared to bare FTO (solid black). The measurements were performed with a three electrode setup using an Ag/AgCl reference electrode and an aqueous $Fe(CN)_6^{3-}$/$Fe(CN)_6^{4-}$ redox electrolyte. (b) Schematic drawing of a FTO/electrolyte interface, showing unhindered electron transfer. (c) A compact $TiO_2$ layer prevents electron transfer when a negative potential is applied to the FTO with respect to the electrolyte.

was replaced by a $TiCl_4$-treated substrate. Further improvement was achieved when the FTO substrate was coated by 20 and 80 nm thick compact $TiO_2$ blocking layer.

A similar trend was observed for ZnS treated QDSCs (Figure 3b), with the difference being that the best performance is achieved for a cell with a 60 nm thick compact $TiO_2$ layer, after which the performance starts to decrease. Figure 3c,d schematically shows the CdSe QDSC without and with the compact layer, the dashed arrows symbolizing recombination of electrons from the $TiO_2$ film with oxidized redox species, while solid arrows depict the recombination path at the FTO/electrolyte interface.

The $J_{sc}$, $V_{oc}$, fill factor, and $\eta$ are shown in Figure 4a−d as a function of the compact $TiO_2$ layer thickness for ZnS treated and untreated cells. The results for $TiCl_4$ treated FTO substrates are plotted at a thickness of 5 nm, which is an estimated average of the patchy $TiO_2$ deposition. For ZnS-free QDSCs, the $J_{sc}$ increases with the compact $TiO_2$ film thickness and reaches a maximum at layer thicknesses up to 100 nm, while at thicker layers, $J_{sc}$ decreases (see Supporting Information Figure S2). The $J_{sc}$ for ZnS-treated QDSCs is in general higher compared to untreated cells with the highest currents for compact layer thickness around 60 nm. The $V_{oc}$ increase of ~40 mV in ZnS free cells does not show any pronounced thickness dependence, while in ZnS-treated devices, the highest $V_{oc}$ is achieved at a compact layer thickness of ~20 nm reaching almost 600 mV. The fill factor, however, does not show any significant changes as a function of the compact layer thickness and fluctuates between 60−62%. Only


dx.doi.org/10.1021/jp306782q | J. Phys. Chem. C 2012, 116, 17473−17478

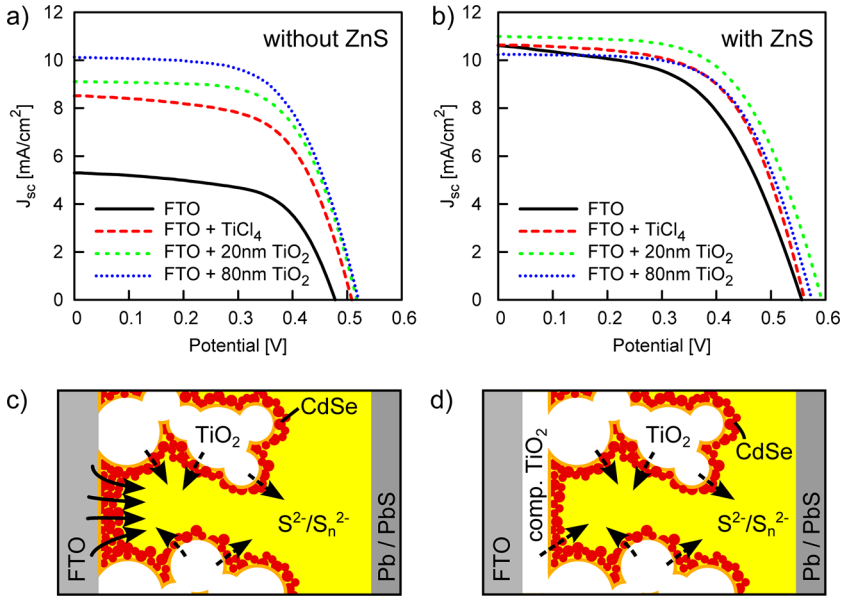


**Figure 3.** (a) $I-V$ characteristics of CdSe QDSCs without ZnS post-treatment showing a cell without FTO surface treatment (solid black), a $TiCl_4$-treated FTO substrate (dashed red), a FTO substrate covered with a 20 nm (short dashed green), and 80 nm thick compact $TiO_2$ layer (dotted blue), preventing direct contact between the FTO with the polysulfide redox electrolyte. (b) Same as that in panel a but for a set of QDSC with ZnS post-treatment. (c) Schematic drawing of a QDSC showing the CdS seeding layer (orange line) and the chemical bath deposited multilayer of CdSe QDs (red dots). Dashed arrows symbolize recombination of electrons with oxidized redox species in the porous film, while solid arrows show the recombination process at the FTO substrate. (d) A compact $TiO_2$ layer covers the FTO substrate and reduces electron recombination.

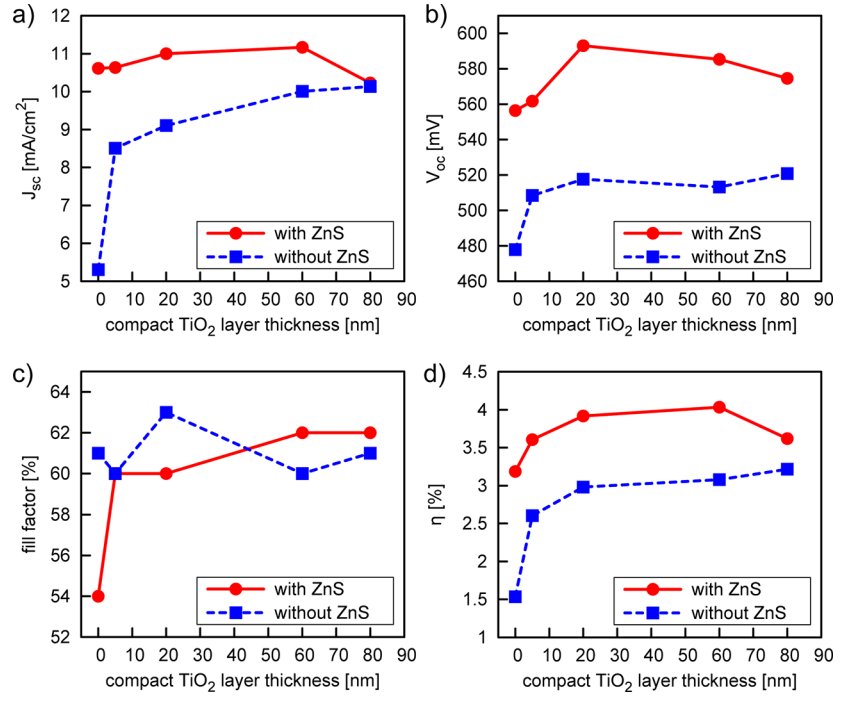


**Figure 4.** (a) Short circuit current density, $J_{sc}$, (b) open circuit voltage, $V_{oc}$, (c) fill factor, and (d) light to electric power conversion efficiency $\eta$ as a function of the compact layer thickness covering the FTO substrate for ZnS post-treated (red circles) and untreated QDSCs (blue squares).

the ZnS-treated reference cell based on an untreated FTO substrate has a lower fill factor of 54%. In ZnS-free QDSCs, the compact $TiO_2$ layer nearly doubles the conversion efficiency from 1.5% to 3.0%, while in ZnS-treated cells, an increase from 3.2% to 4.0% is observed when a compact $TiO_2$ layer of some tens of nanometers covers the FTO substrate.

The results show that, in QDSCs, recombination at the FTO front electrode plays a significant role for the solar cell performance and cannot be neglected like in liquid $I^-/I_3^-$ electrolyte-based DSCs. By covering the FTO substrate, we observe significant changes in the $I-V$ characteristics even though the sensitized porous $TiO_2$ film with its high interface area remains unchanged. In the following, we discuss charge transfer through that interface using a simple equivalent circuit shown in Figure 5a. The equivalent circuit consists of a current source representing charge generation at the $TiO_2$/QD/


dx.doi.org/10.1021/jp306782q | J. Phys. Chem. C 2012, 116, 17473−17478

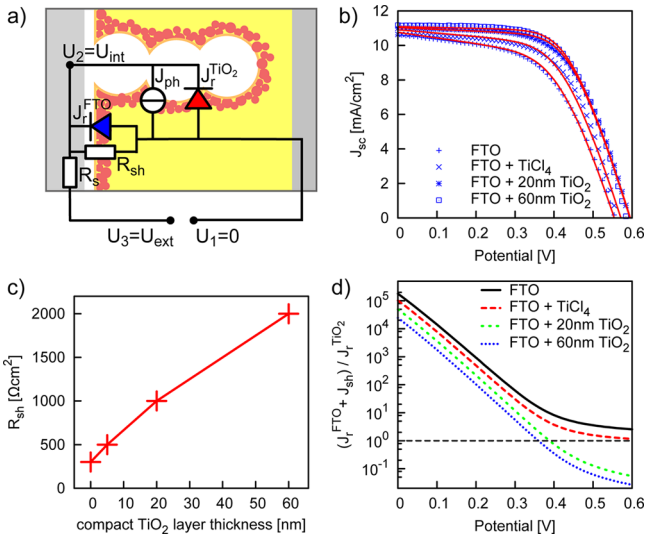


**Figure 5.** (a) Schematic drawing of the equivalent circuit used to calculate the $I-V$ curves. In contrast to standard $PV$ cell representation, two different diodes are representing nonlinear recombination processes, i.e., at the $TiO_2$/electrolyte (red) and FTO/electrolyte interface (blue). (b) Measured (blue symbols) and calculated $I-V$ curves (red solid lines) of the ZnS treated QDSCs. (c) Shunt resistance as a function of the compact layer thickness taken from the calculated $I-V$ curves for ZnS treated cells. (d) Total recombination current at the FTO contact (current through the shunt resistor $J_{sh}$ plus recombination current $J_r^{FTO}$ described by the blue diode) divided by the recombination current at the porous $TiO_2$/electrolyte interface ($J_r^{TiO_2}$, described by the red diode).

electrolyte interface within the porous film ($J_{ph}$), while recombination at the same interface is described by a simple diode equation $J_r^{TiO_2} = J_{r0}^{TiO_2}(\exp(qU_2/n^{TiO_2}k_BT) - 1)$ (diode depicted in red). Recombination at the front contact, however, is represented by a shunt resistor ($R_{sh}$) connected in parallel with a diode $J_r^{FTO} = J_{r0}^{FTO}(\exp(qU_2/n^{FTO}k_BT) - 1)$ (blue diode), accounting for nonlinear charge transfer as a function of applied potential. The reverse bias saturation current densities at the FTO/electrolyte and $TiO_2$/electrolyte interface are $J_{r0}^{FTO}$ and $J_{r0}^{TiO_2}$, respectively, while $n^{FTO}$ and $n^{TiO_2}$ are the ideality factors corresponding to the respective junctions. The elementary charge is denoted by $q$, the Boltzmann constant by $k_B$, the absolute temperature by $T$, and the internal potential at the FTO surface is labeled as $U_2$. Finally, the sheet resistance of the FTO substrate is taken into account by the series resistor $R_s$.

We note that charge transfer at semiconductor electrolyte interfaces is fully described by Marcus–Gerischer theory;[28,29] however, for practical purposes, a simple diode equation can be applied when only a limited potential range is considered. More complex equivalent circuits have been developed based on a network of diodes and resistors to account for the porous $TiO_2$ structure in contact with the redox electrolyte,[30,31] which can be linearized to a transmission line model for impedance spectroscopy analysis.[32] For the investigation of the front contact properties, however, simple equivalent circuits, which are based on the standard photovoltaic cell representation with an adapted front contact have proven to be powerful.[33]

Figure 5b shows the calculated $I-V$ curves (red solid lines) compared to the measured data on ZnS treated cells (same data as in Figure 3b). Table 1 summarizes the parameters of the equivalent circuit elements that were used for the calculated $I-V$ curves. The photocurrent $J_{ph}$, the dark reverse current $J_{r0}^{TiO_2}$, and the ideality factor $n^{TiO_2}$ of the diode describing recombination of electrons from the porous $TiO_2$ with oxidized electrolyte species were kept constant while the parameters describing recombination at the FTO substrate such as $R_{sh}$, $J_{r0}^{FTO}$, and $n^{FTO}$ were changed as a function of the blocking layer thickness. From Table 1, it can be seen that the shunt resistance increases with the compact layer thickness (also shown in Figure 5c), while the nonlinear recombination current described by $J_r^{FTO}$ decreases on $TiCl_4$-treated FTO substrates and is entirely suppressed in QDSCs where the FTO electrode is covered with a compact $TiO_2$ layer deposited by spray pyrolysis. Figure 5d shows the recombination current density at the FTO/electrolyte interface ($J_r^{FTO} + J_{sh}$) divided by the recombination at the $TiO_2$/electrolyte interface ($J_r^{TiO_2}$). Following this analysis, it can be inferred that most of the recombination current occurs at the FTO/electrolyte interface especially at low voltages below the maximum power point ($U_{ext} < 0.4$ V). At voltages between the maximum power point and the $V_{oc}$, one can see the superior behavior of the spray deposited compact $TiO_2$ layers for the suppression of contact recombination at the FTO substrate, which leads to larger photovoltages and an improved fill factor.

We note that this simple model cannot explain the decrease of $J_{sc}$ at thicker blocking layer thickness, and it also fails to predict the strong dependence of $J_{sc}$ as a function of the compact layer thickness for the cells without ZnS treatment (Figure 3a). Thick blocking layers might act as an additional resistor between the mesoporous $TiO_2$ film and the FTO substrate. An electric field within the compact $TiO_2$ layer can create a Schottky[34] or tunnel[35,36] barrier and in thick layers might lead to a drift current that prevents electrons from reaching the FTO substrate.[37]

Thus far, performance limitations of CdSe QDSCs have mainly been discussed in terms of recombination within the porous film.[38] The nature of the semiconductor/electrolyte interface with the CdS seeding layer, the CdSe QD multilayer, and the ZnS coating is very complex, and a number of recombination paths and mechanisms involving trap states in the $TiO_2$ and QDs have been discussed;[17,39,40] however, recombination paths via the FTO substrate are rarely considered. Our results now show that the FTO/electrolyte interface has a strong impact on the $I-V$ characteristics of CdSe QDSCs and an efficiency improvement can be achieved by covering the FTO with a compact $TiO_2$ layer. We note that the effect of the compact layer is more pronounced in QDSCs

**Table 1. Parameters of the Equivalent Circuit Elements Shown in Figure 5a Used to Calculate the $I-V$ Curves of Figure 5b**

| | $J_{ph}$ (mA/cm$^2$) | $R_s$ (Ω cm$^2$) | $R_{sh}$ (Ω cm$^2$) | $J_{r0}^{TiO_2}$ (mA/cm$^2$) | $n^{TiO_2}$ | $J_{r0}^{FTO}$ (mA/cm$^2$) | $n^{FTO}$ |
|---|---|---|---|---|---|---|---|
| FTO | 11.15 | 11 | 300 | $5 \times 10^{-8}$ | 1.2 | $4 \times 10^{-6}$ | 1.5 |
| FTO + $TiCl_4$ | 11.15 | 11 | 500 | $5 \times 10^{-8}$ | 1.2 | $2 \times 10^{-6}$ | 1.5 |
| FTO + 20 nm $TiO_2$ | 11.15 | 11 | 1000 | $5 \times 10^{-8}$ | 1.2 | 0.0 | n/a |
| FTO + 60 nm $TiO_2$ | 11.15 | 11 | 2000 | $5 \times 10^{-8}$ | 1.2 | 0.0 | n/a |


dx.doi.org/10.1021/jp306782q | J. Phys. Chem. C 2012, 116, 17473–17478

without ZnS treatment indicating that the ZnS does not only suppress recombination at the $TiO_2$/electrolyte interface but also prevents electron transfer from the FTO into the electrolyte. We emphasize that surface treatments of the porous $TiO_2$ film before or after QD deposition also affects the FTO substrate and that a beneficial effect of such treatments might originate from the suppression of recombination at FTO substrate rather than improved surface properties of the porous film.

## CONCLUSIONS

We have shown that, in polysulfide electrolyte-based CdSe QD sensitized solar cells, a significant efficiency increase can be achieved when a compact $TiO_2$ layer is deposited in between the mesoporous $TiO_2$ film and the FTO substrate. This provides experimental evidence that recombination of electrons from the FTO with oxidized species of the electrolyte are not negligible in contrast to liquid electrolyte-based DSCs. Using simple equivalent circuits, we show that the observed increase in $V_{oc}$ can be explained by a change of the recombination kinetics at the FTO/electrolyte interface. Furthermore, we observe that the relative improvement in QDSCs without a ZnS post-treatment is higher compared to ZnS treated samples, indicating that the ZnS treatment does not only suppress recombination at the mesoporous $TiO_2$/electrolyte or QD/electrolyte interface but also affects the FTO/electrolyte interface, an effect that has not been considered until now.

## ASSOCIATED CONTENT

### Supporting Information

Dark $I-V$ measurements of the FTO substrate in contact with polysulfide electrolyte are shown for bare FTO and compact $TiO_2$ covered FTO. This material is available free of charge via the Internet at http://pubs.acs.org.

## AUTHOR INFORMATION

### Corresponding Author

*E-mail: sven.ruhle@gmail.com (S.R.); zabana@mail.biu.ac.il (A.Z.).

### Author Contributions

†These authors contributed equally to this work.

### Notes

The authors declare no competing financial interest.

## ACKNOWLEDGMENTS

S.R. acknowledges financial support from the European Union within the FP7 framework (Marie Curie Intra-European Fellowship for Career Development). We thank Udi Nemschitz for support in building the spray pyrolysis scanning system.

## REFERENCES

(1) Rühle, S.; Shalom, M.; Zaban, A. *ChemPhysChem* **2010**, *11*, 2290−2304.
(2) Kamat, P. V. *J. Phys. Chem. C* **2008**, *112*, 18737−18753.
(3) Kongkanand, A.; Tvrdy, K.; Takechi, K.; Kuno, M.; Kamat, P. V. *J. Am. Chem. Soc.* **2008**, *130*, 4007−4015.
(4) Yuan, Y.; Riehle, F.-S.; Gu, H.; Thomann, R.; Urban, G.; Krüger, M. *J. Nanosci. Nanotechnol.* **2010**, *10*, 6041−6045.
(5) Mora-Seró, I.; Bisquert, J. *J. Phys. Chem. Lett.* **2010**, *1*, 3046−3052.
(6) Zhang, Q.; Guo, X.; Huang, X.; Huang, S.; Li, D.; Luo, Y.; Shen, Q.; Toyoda, T.; Meng, Q. *Phys. Chem. Chem. Phys.* **2011**, *13*, 4659−4667.
(7) Radich, J. G.; Dwyer, R.; Kamat, P. V. *J. Phys. Chem. Lett.* **2011**, *2*, 2453−2460.
(8) Palomares, E.; Clifford, J. N.; Haque, S. A.; Lutz, T.; Durrant, J. R. *J. Am. Chem. Soc.* **2002**, *125*, 475−482.
(9) Diamant, Y.; Chappel, S.; Chen, S. G.; Melamed, O.; Zaban, A. *Coord. Chem. Rev.* **2004**, *248*, 1271−1276.
(10) Grinis, L.; Kotlyar, S.; Rühle, S.; Grinblat, J.; Zaban, A. *Adv. Funct. Mater.* **2010**, *20*, 282−288.
(11) Rühle, S.; Greenshtein, M.; Chen, S. G.; Merson, A.; Pizem, H.; Sukenik, C. S.; Cahen, D.; Zaban, A. *J. Phys. Chem. B* **2005**, *109*, 18907−18913.
(12) Yahav, S.; Rühle, S.; Greenwald, S.; Barad, H.-N.; Shalom, M.; Zaban, A. *J. Phys. Chem. C* **2011**, *115*, 21481−21486.
(13) Diguna, L. J.; Shen, Q.; Kobayashi, J.; Toyoda, T. *Appl. Phys. Lett.* **2007**, *91*, 023116−023113.
(14) Lee, Y.-L.; Huang, B.-M.; Chien, H.-T. *Chem. Mater.* **2008**, *20*, 6903−6905.
(15) Mora-Seró, I.; Giménez, S.; Fabregat-Santiago, F.; Gómez, R.; Shen, Q.; Toyoda, T.; Bisquert, J. *Acc. Chem. Res.* **2009**, *42*, 1848−1857.
(16) Giménez, S.; Mora-Seró, I.; Macor, L.; Guijarro, N.; Lana-Villarreal, T.; Gómez, R.; Diguna, L. J.; Shen, Q.; Toyoda, T.; Bisquert, J. *Nanotechnology* **2009**, *20*, 295204.
(17) Guijarro, N.; Campina, J. M.; Shen, Q.; Toyoda, T.; Lana-Villarreal, T.; Gómez, R. *Phys. Chem. Chem. Phys.* **2011**, *13*, 12024−12032.
(18) Cameron, P. J.; Peter, L. M. *J. Phys. Chem. B* **2003**, *107*, 14394−14400.
(19) Cameron, P. J.; Peter, L. M.; Hore, S. *J. Phys. Chem. B* **2004**, *109*, 930−936.
(20) Cameron, P. J.; Peter, L. M. *J. Phys. Chem. B* **2005**, *109*, 7392−7398.
(21) Dittrich, T.; Belaidi, A.; Ennaoui, A. *Sol. Energy Mater. Sol. Cells* **2011**, *95*, 1527−1536.
(22) Tachibana, Y.; Umekita, K.; Otsuka, Y.; Kuwabata, S. *J. Phys. D: Appl. Phys.* **2008**, *41*, 102002.
(23) Kim, J.; Choi, H.; Nahm, C.; Moon, J.; Kim, C.; Nam, S.; Jung, D. R.; Park, B. *J. Power Sources* **2011**, *196*, 10526.
(24) Lee, W.; Yoo, B.; Kim, K.; Lee, D.-K.; Kim, H.; Ko, M. J. *J. Nanosci. Nanotechnol.* **2012**, *12*, 1492−1496.
(25) Greenwald, S.; Rühle, S.; Shalom, M.; Yahav, S.; Zaban, A. *Phys. Chem. Chem. Phys.* **2011**, *13*, 19302−19306.
(26) Gorer, S.; Hodes, G. *J. Phys. Chem.* **1994**, *98*, 5338−5346.
(27) Tachan, Z.; Shalom, M.; Hod, I.; Rühle, S.; Tirosh, S.; Zaban, A. *J. Phys. Chem. C* **2011**, *115*, 6162−6166.
(28) Gerischer, H. *Electrochim. Acta* **1990**, *35*, 1677−1699.
(29) Gerischer, H. *J. Phys. Chem.* **1991**, *95*, 1356−1359.
(30) Burgelman, M.; Grasso, C. *J. Appl. Phys.* **2004**, *95*, 2020−2024.
(31) Minnaert, B.; Grasso, C.; Burgelman, M. *C. R. Chim.* **2006**, *9*, 735−741.
(32) Fabregat-Santiago, F.; Bisquert, J.; Garcia-Belmonte, G.; Boschloo, G.; Hagfeldt, A. *Sol. Energy Mater. Sol. Cells* **2005**, *87*, 117−131.
(33) Kron, G.; Rau, U.; Werner, J. H. *J. Phys. Chem. B* **2003**, *107*, 13258−13261.
(34) Kron, G.; Egerter, T.; Werner, J. H.; Rau, U. *J. Phys. Chem. B* **2003**, *107*, 3556−3564.
(35) Pichot, F.; Gregg, B. A. *J. Phys. Chem. B* **1999**, *104*, 6−10.
(36) Rühle, S.; Cahen, D. *J. Phys. Chem. B* **2004**, *108*, 17946−17951.
(37) Rühle, S.; Dittrich, T. *J. Phys. Chem. B* **2005**, *109*, 9522−9526.
(38) Giménez, S.; Lana-Villarreal, T.; Gómez, R.; Agouram, S.; Munoz-Sanjosé, V.; Mora-Seró, I. *J. Appl. Phys.* **2010**, *108*, 064310−064317.
(39) González-Pedro, V.; Xu, X.; Mora-Seró, I. N.; Bisquert, J. *ACS Nano* **2010**, *4*, 5783−5790.
(40) Hod, I.; González-Pedro, V.; Tachan, Z.; Fabregat-Santiago, F.; Mora-Seró, I.; Bisquert, J.; Zaban, A. *J. Phys. Chem. Lett.* **2011**, *2*, 3032−3035.